

CHEMICAL KINETICS  
AND CATALYSIS

## Low-Temperature Conversion of *ortho*-Hydrogen to *para*-Hydrogen over Ni/Al<sub>2</sub>O<sub>3</sub> Supported Catalysts

A. V. Zhuzhgov<sup>a,\*</sup>, O. P. Krivoruchko<sup>a†</sup>, and L. A. Isupova<sup>a</sup>

<sup>a</sup> Boreskov Institute of Catalysis, Siberian Branch, Russian Academy of Sciences, Novosibirsk, 630090 Russia

\*e-mail: faleks2010@gmail.com

Received December 4, 2018; revised May 14, 2019; accepted June 11, 2019

**Abstract**—Comparative studies of Ni/Al<sub>2</sub>O<sub>3</sub> catalysts during the low-temperature conversion of *ortho*-hydrogen to *para*-hydrogen are performed. Industrial alumina of A-64 grade, obtained via precipitation (OAPP-1), and alumina obtained via thermal activation (without coprecipitation) (OAPP-2), are used as the substrates. The volumetric reaction rate constants of 8 ± 1% Ni/OAPP-1 and 8 ± 1% Ni/OAPP-2 catalysts prepared on the basis of these substrates during low-temperature *ortho*–*para* conversion (OPC) are  $2.2 \times 10^{-3}$  and  $2.4 \times 10^{-3}$  mol cm<sup>-3</sup> s<sup>-1</sup>, respectively, allowing the use of a more environmentally attractive substrate in preparing the catalyst.

**Keywords:** alumina substrates, 8 ± 1% Ni/Al<sub>2</sub>O<sub>3</sub> supported catalysts, reaction of *ortho*–*para* conversion of hydrogen

**DOI:** 10.1134/S0036024419120379

### INTRODUCTION

It is known that hydrogen of normal composition (*n*-H<sub>2</sub>) is a mixture of two modifications, *ortho*-hydrogen (*o*-H<sub>2</sub>) and *para*-hydrogen (*p*-H<sub>2</sub>), which differ by nuclear spins: in *o*-H<sub>2</sub>, the spins of the nuclei are parallel to each other, while *p*-H<sub>2</sub> is characterized by anti-parallel spin [1]. Under normal conditions, gaseous hydrogen contains 75% *o*-H<sub>2</sub> and 25% *p*-H<sub>2</sub>. After the liquefaction of hydrogen with normal composition (at 21–22 K), a slow reaction of OPC spontaneously proceeds in the liquid phase. A heat of conversion is emitted (about 1057 J/mol) that exceeds the characteristic heat of evaporation of liquid hydrogen of 953 J/mol. Uncontrollable losses of liquid hydrogen upon storage and/or transportation occur as a result of high internal heat release [2–4]. According to some estimates, the losses of hydrogen after its liquefaction under normal pressure are around 20% within the first day, and about 50% of the initial volume remains after four days [5–7].

It should be noted that the conversion of *o*-H<sub>2</sub> to *p*-H<sub>2</sub> in both the gas phase and the liquid state is ensured by a catalyst. Without a catalyst, this reaction does not proceed at all in gaseous hydrogen and proceeds slowly in liquid hydrogen. To obtain liquid *p*-H<sub>2</sub>, its liquefaction should therefore be combined with the reaction of *ortho*–*para* conversion in the presence of a catalyst. This task is performed in a reactor that is part

of the integrated system of a hydrogen liquefier at 20–21 K [5, 6].

In [8], we considered problems of preparing liquid *p*-H<sub>2</sub> via the catalytic OPC of gaseous hydrogen of normal composition at cryogenic temperatures, the catalysts for this process, and a number of questions on the operation of these catalysts under the conditions of certain hydrogen liquefiers. The science behind the cryogenic heterogeneous catalytic production of liquid *para*-hydrogen in the Soviet period was reflected in [9].

In 1972, the Institute of Catalysis, Siberian Branch, Academy of Sciences of the Union of Soviet Socialist Republics, developed a series of IK-5 catalysts (IK-5-1, IK-5-2, IK-5-3, and IK-5-4) for OPC, the scaled-up production of which began at the Stalin State Electrochemical Plant in Chirchik, Uzbek Soviet Socialist Republic [9]. The production of liquid cryogenic *p*-H<sub>2</sub>, synthesized using the specified catalyst, began at the same plant. IK-5-4, NiO oxide supported on an industrial alumina substrate of A-1 grade (the one most common back then), was one of the most effective of the developed catalysts [8, 9]. Such advantages as its fairly high activity, ease of preparation, and resistance to deactivation, defrosting, and the cooling of OPC reactors charged with it, contributed to the effectiveness of IK-5-4 catalyst.

The aim of this work was to determine the effect the physicochemical properties of Al<sub>2</sub>O<sub>3</sub> substrates prepared according to different technologies have on the

<sup>†</sup> Deceased.

**Table 1.** Textural characteristics of the initial alumina substrates

Substrate	$d/l$ of granules, mm	$B$ , mL/g	$\gamma$ , g/cm <sup>3</sup>	$S_{sp}$ , m <sup>2</sup> /g	$V_s$ , cm <sup>3</sup> /g	$D$ , nm
OAPP-1	$2.8 \pm 0.2/3 \pm 1$	0.7	0.55	250	0.73	10.5
OAPP-2	$2.0 \pm 0.5/3 \pm 1$	0.4	0.80	283	0.32	4.5

$D$  is the average pore diameter.

activity of Ni/Al<sub>2</sub>O<sub>3</sub> supported catalysts during the conversion of *ortho*-hydrogen into *para*-hydrogen at cryogenic temperatures.

## EXPERIMENTAL

Two types of alumina substrates were used in this work to prepare supported Ni catalysts: alumina of the A-64 grade (TU (Technical Specification) 2163-025-04610600-2003) (OAO Angarsk Plant of Catalysts and Organic Synthesis) and alumina prepared using the product of the centrifugal thermal activation of gibbsite (CTA-GB) [10]. The above substrates were denoted as OAPP-1 (A-64 grade) and OAPP-2 (based on CTA-GB).

Our industrial sample of OAPP-1 had granules with diameters of  $3.0 \pm 0.5$  mm and lengths  $l$  of  $3 \pm 1$  mm. The synthesis of this industrial substrate is based on the traditional means of precipitation (the sol–gel technique) of aqua complexes of Al<sup>3+</sup> from aqueous solution of aluminum sulfate Al<sub>2</sub>(SO<sub>4</sub>)<sub>3</sub> · 9H<sub>2</sub>O (according to sulfate technology).

The procedure for preparing an OAPP-2 substrate according to the thermal activation of a powder of gibbsite (without coprecipitation) consists of preparing the product of thermal activation of gibbsite (GB), its hydration, and extrusion molding. The product of the thermal activation of gibbsite was obtained using a TsEFRAR apparatus according to TU (Technical Specification) 2175-040-03533913-2007. The thermal activation of gibbsite was performed at a temperature of thermal electric heating units of 615°C, a 60 rpm rate of drum rotation, and a 30 kg/h consumption of GB powder. Gibbsite of GD 000 grade (TU (Technical Specification) 1711-99-039-2000) (OAO Achinsk Clay Plant) was used as feedstock for preparing the product of centrifugal thermal activation of GB (CTA-GB).

The OAPP-2 substrate was prepared by hydrating the powder of CTA-GB for 24 h in an acidified aqueous medium at room temperature and a pH of 3.0–3.5. The weight ratio of the solid phase to the solution was 1 : 10. When hydration was complete, the obtained precipitate was separated from the solution via decantation, and the paste was molded using a laboratory syringe with a die hole diameter of 2.5 mm. The factory sample granules with  $d = 2.5$  mm and  $l = 3 \pm$

1 mm were dry-cured for 24 h at room temperature, dried for 6 h at 110°C, and calcinated for 4 h at 550°C. The characteristics of the substrates are presented in Table 1.

The catalysts were prepared via single incipient wetness impregnation of the substrates using aqueous solutions of nickel nitrate Ni(NO<sub>3</sub>)<sub>2</sub> · 6H<sub>2</sub>O. Prior to impregnation, all samples were dried in air 6 h at 110°C for and then calcinated for 4 h at 400 K to protect the surface from possible impurities adsorbed from the atmosphere during storage.

The required concentration of Ni<sup>2+</sup> cations in the impregnating solutions was calculated on the basis of the moisture capacity of the substrates (Table 1) and controlled via the density of the solutions. The total concentration of nickel applied onto each of the substrates was  $8 \pm 1$  wt %, calculated for Ni<sup>2+</sup>. Prior to impregnation, all solutions were subjected to filtration to remove possible particulate matter present in them. The samples were then dry-cured for 24 h in air. Next, drying and thermal treatment in an air flow were done in the stepwise mode 110°C/10 h → 250°C/4 h → 330 ± 5°C/6 h. In all cases, the volume of the impregnating solution was determined by the formula  $V_{sol} = m_{wa}B$  (where  $m_{wa}$  is the weighed amount of the substrate, g;  $B$  is the moisture capacity, mL/g).

**The X-ray diffraction patterns** of the samples were recorded on a D-500 diffractometer (Siemens) using CuK<sub>α</sub> radiation and a graphite monochromator on a reflected beam. The samples were obtained by scanning in the region of angles  $2\theta = 10^\circ$ – $70^\circ$  in increments of 0.05° with an acquisition time of 3 s. The phases were identified by comparing the experimental X-ray diffraction patterns to those of the investigated samples contained in the ICDD database, PDF 2.

**Thermal analysis** was performed on a derivatograph (NETZSCH, Germany) in the range of temperatures from 20 to 1000°C at a 10 K/min rate of heating in an air flow. The thermograms for the supported Ni samples were recorded in a helium flow with a hydrogen concentration of 5 vol %, up to a temperature of 600°C. In all cases, the amount of the investigated sample was 30 mg.

**The morphology** of the samples was studied via high-resolution transmission electron microscopy (HR-TEM) on a JEM-2010 electron microscope at an accelerating potential of 200 kV and a resolving power of 1.4 Å. The samples were deposited on a copper grid

from a suspension in alcohol obtained using an ultrasonic disperser. Local analysis of the elemental composition of the samples was performed using a Phoenix energy dispersive EDAX spectrometer with a Si(Li) detector and energy resolution of about 130 eV.

**The size of the specific surface area ( $S_{sp}$ ,  $m^2/g$ )** was measured from the sorption of argon at 77 K and subsequent thermal desorption according to four points of sorption equilibrium on a SORBI-M 4.1. instrument (ZAO META, Russia) using the soft Sorbi-M Version 4.2 program. Helium was used as the carrier gas in the mixture. The values of  $S_{sp}$  were calculated using the classical Brunauer–Emmett–Teller (BET) approach.

**Elemental chemical analysis** of the supported Ni samples was performed via X-ray fluorescence spectroscopy on an ARL Advant'x analyzer equipped with the Rh anode of an X-ray tube.

**The acid properties** of the samples' surfaces were studied via the IR spectroscopy of adsorbed CO. The IR spectra were recorded on a Shimadzu FTIR-8300 spectrometer in the region of 400–6000  $cm^{-1}$  with a resolution of 4  $cm^{-1}$  and period acquisition of 100 scans. The samples were pressed into tablets  $1 \times 2$   $cm^2$  in size with a weights of 20–40 mg. The tablet was placed in an IR cell and calcinated for 1 h in vacuum at 500°C and a residual gas pressure of at least  $10^{-4}$  Torr. The adsorption of CO was performed in two versions: at  $-196^\circ C$  and CO pressures of 0.1 to 10 Torr, and at room temperature and a CO pressure of 10 Torr. The concentrations of the Lewis acid sites (LASs) and Brønsted acid sites (BASs) were determined from the characteristic intensities of the observed characteristic absorption bands using integral absorption coefficients.

**The catalytic activity** of Ni catalysts in the OPC reaction was determined on a flow-type unit at 10 atm and 77 K. Electrolytic  $H_2$ , preliminarily purified of potential  $H_2O$  impurities using a zeolite of CaA-Y(5) grade, impurities of nitrogen and  $CO_x$  on a column with activated charcoal of AG-3 grade at liquid nitrogen temperature, and microimpurities of  $O_2$  on an aluminum–nickel catalyst, was used in this work. The investigated samples in the form of granules and fractions (0.25–0.5 mm) with a volume of 3  $cm^3$  was charged into the reactor and then activated for 4 h at  $110^\circ C$  in a dried hydrogen flow, fed in at rates of 60–70 L/h to remove weakly bound molecular water from the catalyst, and then for 4 h at  $250^\circ C$  to reduce it. After activation, the reactor with the catalyst was cooled to room temperature and then immersed in a Dewar vessel filled with liquid nitrogen. During measurements, the reactor was constantly cryostatted with liquid nitrogen, and a pressure of 10 atm was main-

tained. The flow rates of hydrogen were varied in the range of 200 to 900 L/h during measurements.

The activity of the catalysts was characterized by first-order volume or weight reaction rate constants, according to Eqs. (1) and (2), respectively [28, 30]:

$$k_v = \frac{n}{V} \ln \frac{1 - C_0/C_{eq}}{1 - C/C_{eq}} \text{ mol cm}^{-3} \text{ s}^{-1}, \quad (1)$$

$$k_w = \frac{n}{m} \ln \frac{1 - C_0/C_{eq}}{1 - C/C_{eq}} \text{ mol g}^{-1} \text{ s}^{-1}, \quad (2)$$

where  $n$  is the consumption of hydrogen (productivity), mol/s, which is set and adjusted during each experiment;  $k_v$  is the volumetric reaction rate constant,  $\text{mol cm}^{-3} \text{ s}^{-1}$  (or, allowing for bulk density,  $\text{mol g}^{-1} \text{ s}^{-1}$ );  $V_c$  is the volume of the catalyst,  $\text{cm}^3$ ;  $m_c$  is the weight of the weighed amount, g;  $\gamma_c$  is the bulk density of the catalyst,  $\text{g/cm}^3$ ; and  $C_0$ ,  $C_{eq}$ , and  $C$  are the initial, equilibrium, and obtained concentrations of  $p\text{-H}_2$ , respectively. Detailed calculations of the rate constants using Eqs. (1) and (2) were presented in [5].

## RESULTS AND DISCUSSION

Our studies of the textural characteristics of the investigated substrates presented in Table 1 testify to the substantial differences that must be considered in preparing supported catalysts. The substrates differ by their total pore volumes and moisture capacities, and by the average pore sizes at close values of the specific surface area. This shows that in the OAPP-1 substrate, the main contribution to the surface is made by the surfaces of mesopores; in the OAPP-2 substrate, by the surfaces of micropores.

The substrates also differ by phase composition. The diffraction patterns of our (a) industrial and (b) original substrates presented in Fig. 1 correspond to the low-temperature modification of  $\gamma\text{-Al}_2\text{O}_3$  (OAPP-1) and a  $\gamma\text{-Al}_2\text{O}_3 + \eta\text{-Al}_2\text{O}_3$  mixture (OAPP-2). The positions of the reflections and the set of interplanar distances of these samples correspond to  $\gamma\text{-Al}_2\text{O}_3$  and  $\eta\text{-Al}_2\text{O}_3$  obtained by calcinating well-crystallized boehmite and bayerite for 6 h at  $550^\circ C$  (Fig. 1c). The results are in agreement with the ICDD database, PDF 2; 00-0-33-0018, 00-0-21-1307.

The different conditions of preparing the substrates also affect the acid properties of the surface, which can play an important role in both the preparation of supported catalysts and possibly the process of OPC. We therefore studied the acid sites of surfaces via IR spectroscopy of adsorbed CO molecules of the initial  $\text{Al}_2\text{O}_3$  substrates and Ni catalysts obtained on their basis.

Absorption bands in the range of 1300–1700  $cm^{-1}$  that characterize stretching vibrations in carbonate and carboxylate structures are observed in the IR spectra of all the initial substrates (Fig. 2a, 1–3).

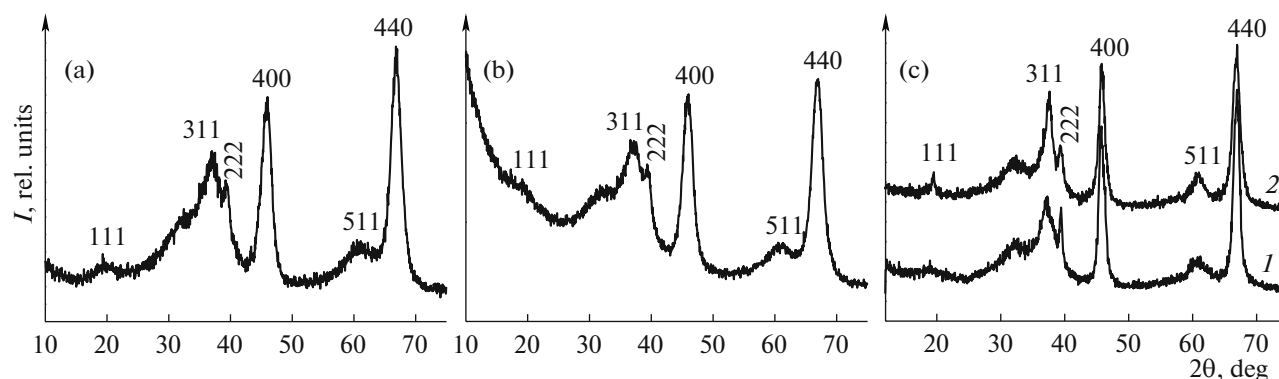


**Fig. 1.** X-ray diffraction patterns of industrial OA substrates and reference samples: (a) OAPP-1, (b) OAPP-2, and (c) reference samples: (1)  $\gamma$ - $\text{Al}_2\text{O}_3$  and (2)  $\eta$ - $\text{Al}_2\text{O}_3$ .

Absorption bands at  $1350$ – $1380$  and  $1590$   $\text{cm}^{-1}$  belong to the symmetric and asymmetric stretching vibrations of  $\text{COO}^-$  in the structure of carboxylate, respectively. Absorption bands at  $1460$   $\text{cm}^{-1}$  correspond to the asymmetric stretching vibrations of  $\text{C}-\text{O}$  in the struc-

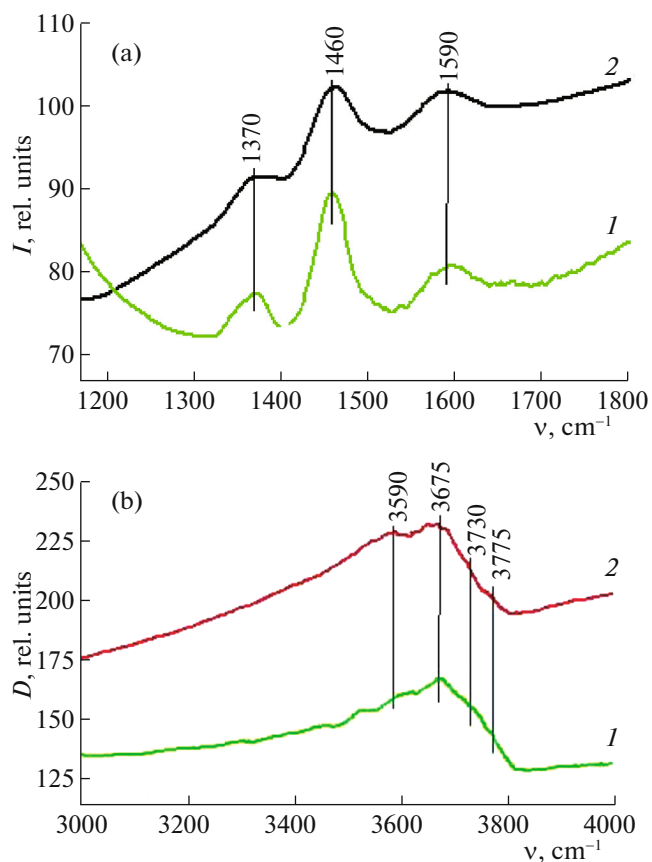


**Fig. 2.** (Color online) (a) IR spectra of the (1) OAPP-1 and (2) OAPP-2 substrates in the region of vibrations of the carbonate groups and molecular water. (b) Region of stretching vibrations of the OH groups: (1) OAPP-1 and (2) OAPP-2.

ture of monodentate carbonate, which normally forms when atmospheric  $\text{CO}_2$  interacts with the basic sites of the surface ( $\text{O}^{\delta-}$  ions) [11, 12].

In the region of the stretching vibrations of OH groups (Fig. 2b), the samples of the substrates are characterized by the absorption bands at  $3590$ ,  $3675$ ,  $3730$ , and  $3775$ – $3780$   $\text{cm}^{-1}$  that are typical of low-temperature modifications of aluminas [13]. The absorption band at  $3590$   $\text{cm}^{-1}$  belongs to the H-bound hydroxyl groups. The absorption bands at  $3675$  and  $3730$   $\text{cm}^{-1}$  characterize the bridge hydroxyl groups ( $\text{Al}-\text{OH}-\text{Al}$ ), and the absorption band at  $3775$   $\text{cm}^{-1}$  belongs to the OH groups of pentacoordinated aluminum atoms [12, 13].

In our spectra (Figs. 2a, 2b), the intensities of the absorption bands for OAPP-2 are notably higher in the region of vibrations of carbonate and hydroxyl groups, testifying to the higher saturation of the surface of this substrate by both basic sites and BASs, relative to OAPP-1.

Figure 3 presents the IR spectra of CO adsorbed on the substrates at liquid nitrogen temperature ( $77$  K) and  $0.1$ – $10$  Torr. The absorption bands at  $2154$ – $2157$   $\text{cm}^{-1}$  are due to the adsorption of CO on the OH groups (Brønsted acid sites, or BASs). The shift of the absorption bands of the hydroxyl groups upon the adsorption of CO is  $190$ – $195$   $\text{cm}^{-1}$ , which corresponds to the strength of these sites of  $1240$ – $1245$  kJ/mol on the proton affinity scale [11]. Absorption bands at  $2169$ – $2203$   $\text{cm}^{-1}$  belong to CO adsorbed on aluminum cations (LASs) [11].

The parameters of the acid sites of the surfaces of alumina substrates, based on the data from IR spectroscopy, are summarized in Table 2. It is seen from our results that OAPP-1 is characterized by a somewhat higher concentration of BASs (the absorption band at  $2155$ – $2157$   $\text{cm}^{-1}$ ). The substantial difference

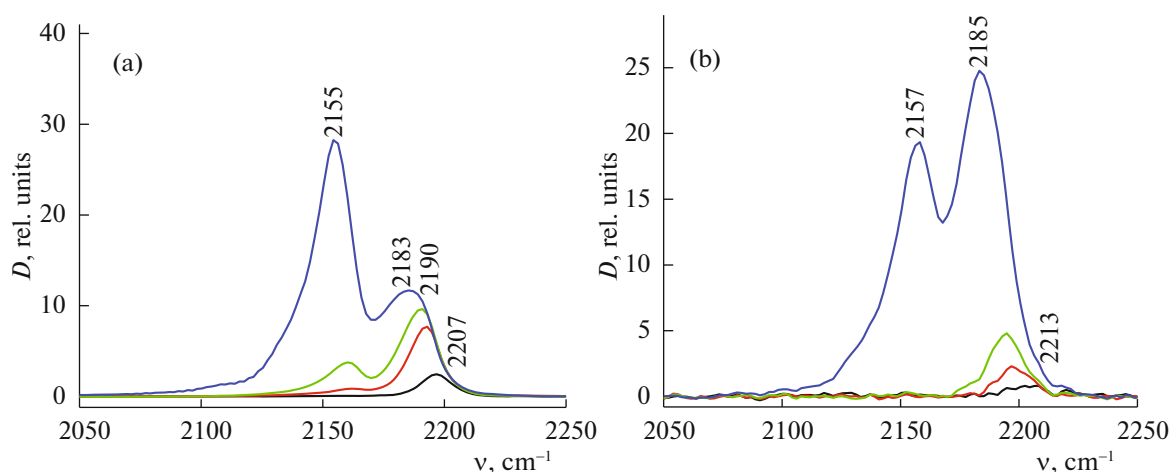


**Fig. 3.** (Color online) IR spectra of CO adsorbed on the substrates at 77 K and a pressure from 0.1 to 10 Torr: (a) OAPP-1 and (b) OAPP-2.

between the substrates is apparent from the concentration of LASs on the substrate based on CTA-GB (OAPP-2) exceeding the one for the industrial OAPP-1 sample by more than 200%.

Notable differences in the phase composition, textural characteristics, and acid properties of the surfaces of the OAPP-1 and OAPP-2 substrates were thus revealed. They were due to differences between the procedures of their preparation.

In the X-ray diffraction patterns of the factory sample Ni catalysts with a total nickel content of  $8 \pm 1$  wt % (calculated for  $\text{Ni}^{2+}$ ), only peaks that belong to the corresponding  $\text{Al}_2\text{O}_3$  substrate are observed (Fig. 4, 1–3). This shows the particles of nickel oxide formed on the surfaces of the substrates should be no larger than 3–4 nm [14]. According to the HR-TEM data (Fig. 5), virtually cluster accumulations of nickel oxide particles with sizes of around 3 nm are observed in the high-resolution electron microscope images of the samples of  $8 \pm 1\%$  Ni/OAPP-1 and  $8 \pm 1\%$  Ni/OAPP-2 catalysts, which can be recorded by weak variation in the range of contrast. The areas of

their localization are shown by arrows in the images. Note that the amount of supported  $\text{Ni}^{2+}$  ( $8 \pm 1\%$ ) was chosen based on this particular concentration of the active component providing the maximum activity of this type of catalysts in the reaction of OPC, according to [15, 16].

It is known that calcinating  $\text{NiO}/\text{Al}_2\text{O}_3$  supported catalysts above  $350^\circ\text{C}$  leads to NiO interacting with the alumina substrate, followed by the formation of pseudospinel structures of the  $\text{NiAl}_2\text{O}_4$  type. This raises the temperature of activation of the catalyst in a hydrogen flow, since nickel aluminates are compounds that are hard to reduce [17, 18]. On the other hand, ultradisperse nickel oxide particles with sizes of around 1 nm form upon calcinating the catalysts at  $300^\circ\text{C}$  or temperatures near the decomposition of the supported salt  $\text{Ni}(\text{NO}_3)_2 \cdot 6\text{H}_2\text{O}$  ( $230\text{--}250^\circ\text{C}$ ) [18–20]. Ultradisperse nickel oxide is too sensitive to poisoning by the water vapors present in hydrogen. The optimum temperature of preparing supported Ni catalysts should be in the range of  $300\text{--}350^\circ\text{C}$ . Under these conditions of thermal treatment, we found no

**Table 2.** Characteristics of the acid sites of the initial substrates according to the data of the IR spectra of adsorbed CO

Sample	Absorption band of CO, $\text{cm}^{-1}$	Site type	C, $\mu\text{mol/g}$	$\Sigma\text{LASs}$ and $\text{BASs}$ , $\mu\text{mol/g}$ ( $\mu\text{mol/m}^2$ )
OAPP-1	2155	BAS	96	96 (0.38)
	2183	LAS	283	
	2190	LAS	31	321 (1.28)
	2207	LAS	7	
OAPP-2	2157	BAS	78	78 (0.27)
	2185	LAS	689	
	2213	LAS	17	706 (2.50)

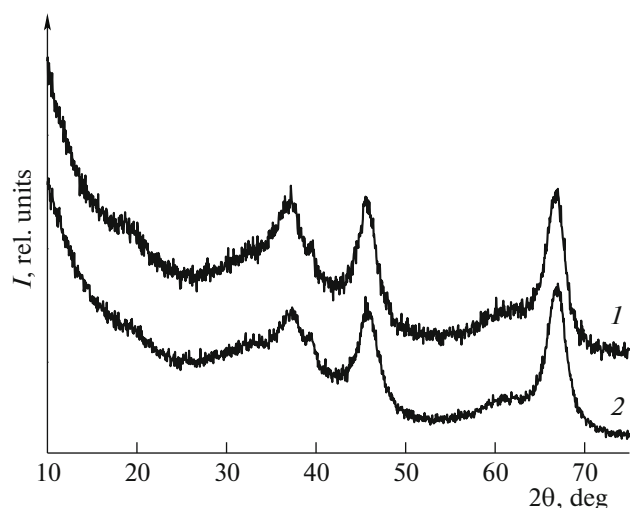


**Fig. 4.** X-ray diffraction patterns of NiO/Al<sub>2</sub>O<sub>3</sub> supported catalysts: (1) 8 ± 1% Ni/OAPP-1 and (2) 8 ± 1% Ni/OAPP-2.

compounds with the structure of spinel NiAl<sub>2</sub>O<sub>4</sub> in the final NiO/Al<sub>2</sub>O<sub>3</sub>, based on the XRD and HR-TEM data. This is also confirmed by Ni<sup>2+</sup> cations on the surface of Al<sub>2</sub>O<sub>3</sub> being stabilized only in the octahedral

oxygen coordination of the NiO phase [19] under our specified conditions of preparation. Nickel oxide was therefore apparently in a highly disperse state on both versions of the substrate. As noted above, this follows from the XRD and HR-TEM data.

The maximum activity of nickel catalysts in the low-temperature reaction of OPC is achieved after its reduction (activation) in a hydrogen flow. The activation and kinetics of reduction of supported nickel catalysts with a similar (8 ± 1 wt %) concentration of active component NiO were studied in some detail in [17, 18]. It was shown that the degree of the catalysts' reduction in a hydrogen flow at 300–320°C was 40–47%. The initial temperature of reduction was 130–140°C, and the final temperature is 300°C. The use of new substrates can affect the reducibility of the prepared catalysts.

Figure 6 presents the data from our thermal analysis of the samples of 8 ± 1% Ni/OAPP-1 and 8 ± 1% Ni/OAPP-2 catalysts, obtained in an atmosphere of 95% He and 5% H<sub>2</sub>. Four types of heat effects—endothermic effects at 80–96°C, caused by the removal of weakly bound water; exo-effects with the maxima at 130 and 140°C associated with the reduction of highly disperse NiO crystallites on the surfaces of the substrates; an intermediate region of reduction

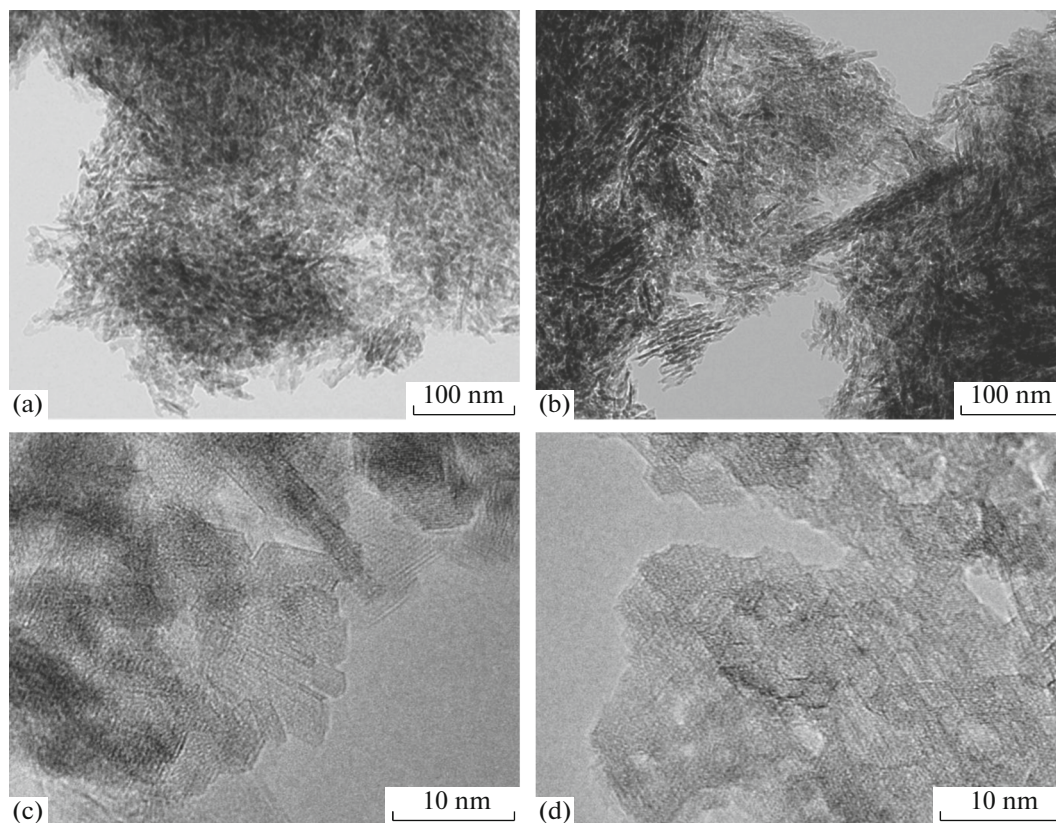


**Fig. 5.** Morphology of the NiO/Al<sub>2</sub>O<sub>3</sub> catalysts: (a) 8 ± 1% Ni/OAPP-1 and (b) 8 ± 1% Ni/OAPP-2.

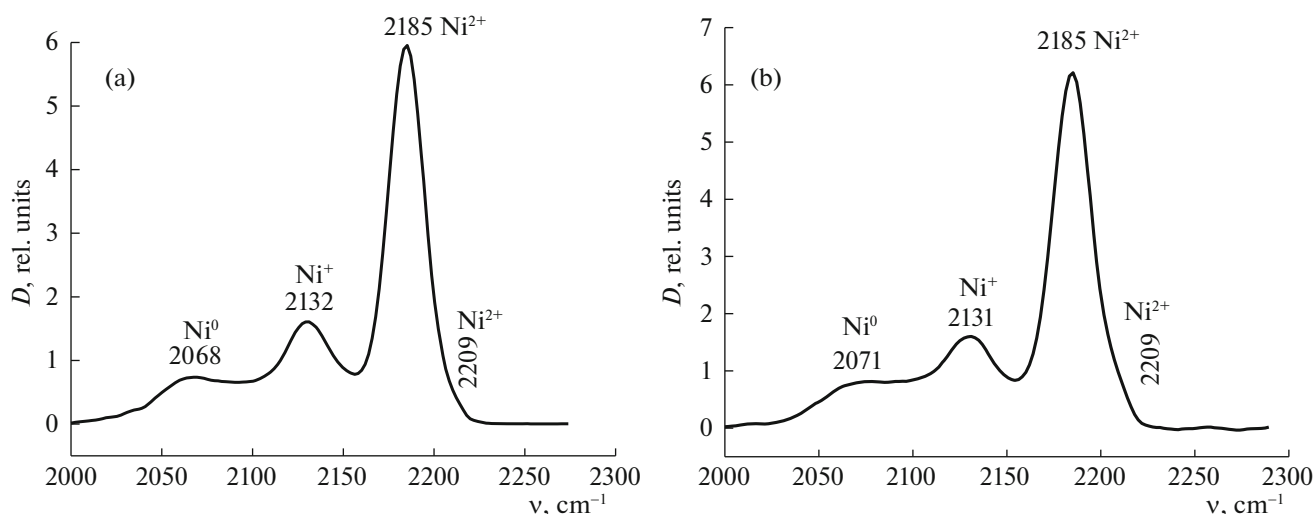


**Fig. 6.** IR spectra of CO adsorbed at room temperature on the surface of preliminarily reduced catalysts: (a)  $8 \pm 1\%$  Ni/OAPP-1 and (b)  $8 \pm 1\%$  Ni/OAPP-2.

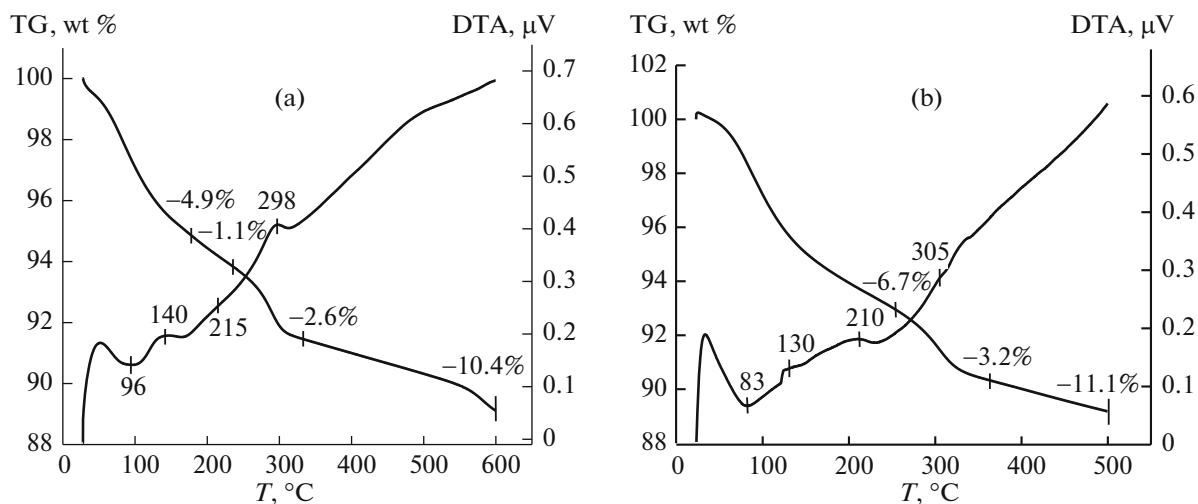


**Fig. 7.** Thermograms of the NiO/Al<sub>2</sub>O<sub>3</sub> catalysts obtained in a medium of 95% He + 5% H<sub>2</sub>: (a)  $8 \pm 1\%$  Ni/OAPP-1 and (b)  $8 \pm 1\%$  Ni/OAPP-2.

at 210–215°C; and an exothermic heat effect with a maximum at about 300°C, which indicates the full completion of the reduction of NiO—are observed in the thermograms of the samples (Fig. 7). Note that the observed range of catalyst reduction corresponds to the one determined earlier. Certain differences in the samples with respect to the data from thermal analysis are observed in the weight losses (LOI). The total weight losses for NiO/OAPP-1 and NiO/OAPP-2 were 10.4 and 11.1 wt %, respectively. In the region of reduction at 300°C, the weight losses are 0.6 wt % higher for Ni/OAPP-2 than for the first catalyst (Fig. 7). These differences in the data of TA are reflected in the degree of NiO reduction in the corresponding temperature regions. The data on the degree

of reduction of Ni catalysts are summarized in Table 3 below. It is seen that for the NiO/OAPP-2 catalyst, the degree of NiO reduction is somewhat higher than with the NiO/OAPP-1 catalyst in all of the observed temperature regions (Table 3), which can be determined for the same particle size from the different degrees of interaction between the nickel oxide particles and the substrates with notably different concentrations of LASs.

The somewhat better reducibility of the NiO/OAPP-2 catalyst is also demonstrated by the data of IR spectroscopy of adsorbed CO. Figure 6 presents the IR spectra of CO adsorbed at room temperature and 10 Torr. Note that at liquid nitrogen temperature, the adsorption of CO proceeds on both

**Table 3.** Temperatures and degrees of reduction of Ni catalysts

Sample	$\alpha_{\text{NiO}}, \%$	$T_{\text{red}}, ^\circ\text{C}$
$8 \pm 1\%$ Ni/OAPP-1	20	150
	25	250
	35	300
	43	600
$8 \pm 1\%$ Ni/OAPP-2	22	150
	27	250
	40	300
	46	600

nickel oxide and the acid sites of the substrate ( $\text{Al}^{3+}$  cations) [11, 12], due to which the experiments were performed at room temperature. Under these conditions, CO is adsorbed mainly on nickel cations. Four almost identical absorption bands with maxima at 2068, 2132, 2184, and 2209  $\text{cm}^{-1}$  are observed on the surfaces of the samples of  $8 \pm 1\%$  Ni/OAPP-1 and  $8 \pm 1\%$  Ni/OAPP-2. The absorption band at 2068  $\text{cm}^{-1}$  belongs to the linear complexes of metallic nickel with CO, the absorption band at 2132  $\text{cm}^{-1}$  characterizes the adsorption of CO on  $\text{Ni}^+$  cations, and the bands at 2184 and 2209  $\text{cm}^{-1}$  characterize the adsorption of CO on  $\text{Ni}^{2+}$  cations. The strength and concentration of the sites were calculated using the equations presented in [11]. The results from our calculations are summarized in Table 4. It is seen that the surface of nickel oxide supported on different substrates is characterized by about the same set of LASs and the strengths of these sites.

Note that according to the IR spectroscopy data, the amount of the reduced forms of nickel ( $\text{Ni}^+$  and

$\text{Ni}^0$ ) in the NiO/OAPP-2 catalyst is somewhat higher than in the NiO/OAPP-1 catalyst, agrees with the data from our thermal analysis of the catalysts in a reducing medium (7%). However, this difference can be offset by the error allowed in the means of analysis themselves.

Table 5 presents the results from studying the activity of the catalysts in the reaction of OPC at liquid nitrogen temperature. It is seen from the data that the activity of the catalyst samples, determined for the fraction (0.25–0.5 mm), is about 200% higher than for the granules. This testifies to the OPC reaction occurring in the region of internal diffusion upon moving from the fraction to the industrial grain, and is in good agreement with the literature data [4–6].

The somewhat lower catalytic activity (per unit weight) for the fraction of the catalyst based on the OAPP-2 substrate at the same concentration of the active component could be due to the higher concentration of LASs on its surface, since the degree of dispersion (according to the XRD and TEM data), the degree of interaction between the active component and the different substrates (according to the TA data), and the properties of the surface (the IR of adsorbed CO) are quite close. At the same time, the activity of the granulated layer of the catalyst (per unit volume of the layer) is somewhat higher for the OAPP-2 substrate than for NiO/OAPP-1, despite the smaller pore size, which reduces the rate of granule utilization. This is due on the one hand to the smaller size of the granules, and to the higher bulk density of the catalyst based on the OAPP-2 substrate on the other.

## CONCLUSIONS

Our two types of  $\text{Al}_2\text{O}_3$  substrate obtained via precipitation and the CTA of gibbsite differed notably with respect to a series of physicochemical characteristics: phase composition, size of the specific surface

**Table 4.** Characteristics of different sites, according to the IR spectra of CO adsorbed on nickel in different states of oxidation

Sample	Absorption band of CO, $\text{cm}^{-1}$	Site type	$C, \mu\text{mol/g}$	$Q_{\text{CO}}, \text{kJ/mol}$
$8 \pm 1\%$ Ni/OAPP-1	2068	$\text{Ni}^0\text{-CO}$	3.7	–
	2132	$\text{Ni}^+\text{-CO}$	6.7	–
	2185	$\text{Ni}^{2+}\text{-CO}$	15.0	22
	2209	$\text{Ni}^{2+}\text{-CO}$	0.4	63
$8 \pm 1\%$ Ni/OAPP-2	2071	$\text{Ni}^0\text{-CO}$	4.0	–
	2131	$\text{Ni}^+\text{-CO}$	7.2	–
	2185	$\text{Ni}^{2+}\text{-CO}$	16.2	22
	2209	$\text{Ni}^{2+}\text{-CO}$	0.9	63



**Table 5.** Data on the activity of the Ni catalysts in the reaction of OPC at 77 K

Sample	$S_{sp}$ , m <sup>2</sup> /g	$k_v \times 10^{-3}$ , mol cm <sup>-3</sup> s <sup>-1</sup>		$k_w \times 10^{-3}$ , mol g <sup>-1</sup> s <sup>-1</sup>		$T_{activation}$ , °C
		fraction	granules	fraction	granules	
8 ± 1% Ni/OAPP-1	217	1.25	0.6	1.6	0.8	150
		4.5	2.2	6.3	3.1	250
8 ± 1% Ni/OAPP-2	240	1.5	0.7	1.4	0.71	150
		4.7	2.4	4.5	2.3	250

area, moisture capacity, bulk density, and the acid properties of the surfaces (the concentrations of LASs and BASs). Based on the considered substrates, we believe it is possible to prepare granulated catalysts with activity similar to that of a unit of a catalyst layer, which is important for practical applications.

Note that from a practical viewpoint, it is quite possible to prepare Al<sub>2</sub>O<sub>3</sub> substrates according to the low-waste technology of the CTA of gibbsite for the subsequent preparation of supported Ni catalysts for OPC that are not inferior to the earlier generation of IK-5-4 catalyst based on an A-1 substrate, in terms of its final characteristics.

#### FUNDING

This work was performed as part of a State Task for the Borekov Institute of Catalysis, Siberian Branch, Russian Academy of Sciences, project AAAA-A17-117041710090-3.

#### REFERENCES

1. A. Farkas, *Orthohydrogen, Parahydrogen, and Heavy Hydrogen* (Cambridge Univ. Press, Cambridge, 1935).
2. R. A. Buyanov, A. G. Zel'dovich, and Yu. K. Pilipenko, *Khim. Prom-st'*, No. 2, 31 (1961).
3. R. A. Buyanov, A. G. Zel'dovich, and Yu. K. Pilipenko, *Gryogenics* **2**, 143 (1962).
4. R. A. Buyanov, A. G. Zel'dovich, and Yu. K. Pilipenko, *Prib. Tekh. Eksp.*, No. 2, 188 (1961).
5. R. A. Buyanov, *Kinet. Katal.* **1**, 306 (1960).
6. R. A. Buyanov, *Kinet. Katal.* **1**, 418 (1960).
7. R. A. Buyanov, *Kinet. Katal.* **1**, 617 (1960).
8. A. V. Zhuzhgov, O. P. Krivoruchko, L. A. Isupova, O. N. Mart'yanov, and V. N. Parmon, *Catal. Ind.* **10**, 9 (2018).
9. R. A. Buyanov and V. N. Parmon, *Katal. Prom-sti*, No. 5, 390 (2017).
10. Yu. Yu. Tanashev, E. M. Moroz, L. A. Isupova, A. S. Ivanova, G. S. Litvak, Yu. I. Amosov, N. A. Rudina, A. N. Shmakov, A. G. Stepanov, I. V. Kharina, E. V. Kul'ko, V. V. Danilevich, V. A. Balashov, V. Yu. Kruglyakov, I. A. Zolotar'skii, and V. N. Parmon, *Kinet. Catal.* **48**, 153 (2007).
11. E. A. Paukshtis and E. N. Yurchenko, *Russ. Chem. Rev.* **52**, 242 (1983).
12. E. A. Paukshtis, *Heterogeneous Acid-Base Catalysis Infrared Spectroscopy* (Nauka, Novosibirsk, 1992), p. 254 [in Russian].
13. A. A. Tsyganenko and K. S. Smirnov, *Mater. Chem. Phys.* **26**, 35 (1990).
14. G. D. Chukin, *The Structure of Alumina and Hydrodesulfurization Catalysts. Reaction Mechanisms* (Paladin, Printa, Moscow, 2010) [in Russian].
15. R. A. Buyanov, O. P. Krivoruchko, V. V. Malakhov, et al., *Kinet. Katal.* **10**, 894 (1969).
16. O. P. Krivoruchko and R. A. Buyanov, *Kinet. Katal.* **13**, 1050 (1972).
17. S. P. Noskova, M. S. Borisova, V. A. Dzis'ko, et al., *Kinet. Katal.* **15**, 592 (1974).
18. S. P. Noskova, M. S. Borisova, and V. A. Dzis'ko, *Kinet. Katal.* **16**, 497 (1975).
19. V. A. Dzis'ko, S. P. Noskova, M. S. Borisova, et al., *Kinet. Katal.* **15**, 751 (1974).
20. M. S. Borisova, B. N. Kuznetsov, V. A. Dzis'ko, et al., *Kinet. Katal.* **16**, 1028 (1975).

Translated by E. Boltukhina